AMERICAN SOCIETY FOR MICROBIOLOGY | Infection and Immunity

Trypanosoma cruzi Causes Paralyzing Systemic Necrotizing Vasculitis Driven by Pathogen-Specific Type I Immunity in Mice

Ester Roffê,[a]* Ana Paula M. P. Marino,[a]* Joseph Weaver,[a] Wuzhou Wan,[a] Fernanda F. de Araújo,[b]* Victoria Hoffman,[c] Helton C. Santiago,[d]* Philip M. Murphy[a]

Molecular Signaling Section, Laboratory of Molecular Immunology, National Institute of Allergy and Infectious Diseases (NIAID), National Institutes of Health (NIH), Bethesda, Maryland, USA[a]; Laboratory of Emerging Pathogens, Division of Emerging and Transfusion Transmitted Diseases, Center for Biologics Evaluation and Research, U.S. Food and Drug Administration, Silver Spring, Maryland, USA[b]; Division of Veterinary Resources, Office of Research Services, Office of the Director, NIH, Bethesda, Maryland, USA[c]; Helminth Immunology Section, Laboratory of Parasitic Diseases, NIAID, NIH, Bethesda, Maryland, USA[d]

Infectious agents are often considered potential triggers of chronic inflammatory disease, including autoimmunity; however, direct evidence is usually lacking. Here we show that following control of acute infection of mice with the myotropic Colombiana strain of *Trypanosoma cruzi*, parasites persisted in tissue at low levels associated with development of systemic necrotizing vasculitis. Lesions occurred in many but not all organs and tissues, with skeletal muscle arteries being the most severely affected, and were associated with myositis, atrophy, paresis/paralysis, and death. Histopathology showed fibrinoid vascular necrosis, rare amastigote nests within skeletal muscle myocytes, and massive leukocyte infiltrates composed mainly of inflammatory monocytes, F4/80$^+$ macrophages, and *T. cruzi* tetramer-specific CD8$^+$ T lymphocytes capable of producing gamma interferon (IFN-γ) and tumor necrosis factor alpha (TNF-α) but not interleukin-17 (IL-17). *T. cruzi*-specific IgG was detected in sera from infected mice, but antibody deposits and neutrophilic inflammation were not features of the lesions. Thus, *T. cruzi* infection of mice may be a specific infectious trigger of paralyzing systemic necrotizing vasculitis most severely affecting skeletal muscle, driven by pathogen-specific type I immune responses.

Vasculitis is a general term for a spectrum of diseases involving leukocyte infiltration of the blood vessel wall. Many subtypes of vasculitis are recognized based on the types of blood vessels involved and the nature of the underlying immunopathology. In some cases, an association of vasculitis with specific infectious agents has been reported; for example, polyarteritis nodosa (PAN) has been associated with hepatitis B virus (HBV), hepatitis C virus (HCV), and HIV infections (1). However, it has been difficult to establish either causality or pathogenetic mechanisms, in part because of the low prevalence of vasculitis and the lack of good animal models (2). In this regard, while studying the chronic phase of C57BL/6J mice infected with the myotropic Colombiana strain of *Trypanosoma cruzi*, the infectious cause of Chagas' disease in humans, we noticed that the majority of animals developed hind limb paralysis associated with severe systemic necrotizing vasculitis affecting arteries and arterioles in skeletal muscle. Lesions were also present in many other tissues. A review of the literature identified several studies from 1970 to 2000 that described perivascular inflammation and frank arteritis in chronically *T. cruzi*-infected mouse skeletal muscle, aorta, nerves, and heart (3–9); however, the underlying immunologic mechanisms of disease were not defined. Interestingly, Okumura et al. reported necrotizing arteritis in small arteries beneath the peritoneal lining of the bowel and, occasionally, of the aorta and coronary arteries of *T. cruzi*-infected mice, which was at that time interpreted as "allergic necrotizing angiitis" (10). Dias et al. reported obliterative changes of the small and medium-sized branches of coronary arteries, with reductions of the vascular lumens, present in younger age groups of autopsied cases of Chagas' disease patients (11).

Here we report an analysis of the clinical, pathological, microbiologic, immunologic, and molecular features of chronic *T. cruzi*-induced systemic necrotizing vasculitis in mice, focusing mainly on skeletal muscle, where the pathology is the most severe. We demonstrate that the lesions are associated with a pathogen-specific type I immune response. This model may be useful for understanding how a specific infectious agent may trigger vasculitis, as well as for understanding the myopathy that occurs in some patients with Chagas' disease (12, 13).

MATERIALS AND METHODS

Animals and parasite. Wild-type male C57BL/6J mice were obtained from the Jackson Laboratory (Bar Harbor, ME). Mice were infected at 8 to 10 weeks of age and were housed in cages under specific-pathogen-free conditions. The myotropic Colombiana strain of *Trypanosoma cruzi* (14, 15), obtained from Fuyuki Tokumasu (Laboratory of Malaria and Vector Research, NIAID, NIH), was maintained by serial passages in Swiss Web-

Received 10 December 2015 **Returned for modification** 15 January 2016
Accepted 26 January 2016

Accepted manuscript posted online 8 February 2016

Citation Roffê E, Marino APMP, Weaver J, Wan W, de Araújo FF, Hoffman V, Santiago HC, Murphy PM. 2016. *Trypanosoma cruzi* causes paralyzing systemic necrotizing vasculitis driven by pathogen-specific type I immunity in mice. Infect Immun 84:1123–1136. doi:10.1128/IAI.01497-15.

Editor: J. A. Appleton

Address correspondence to Philip M. Murphy, pmm@nih.gov.

* Present address: Ester Roffê, Laboratório de Imunologia Celular e Molecular, Centro de Pesquisas René Rachou, Fundação Oswaldo Cruz, Belo Horizonte, MG, Brazil; Ana Paula M. P. Marino, Laboratório de Imunopatologia, Centro de Pesquisas René Rachou, Fundação Oswaldo Cruz, Belo Horizonte, MG, Brazil; Fernanda F. de Araújo, Laboratório de Biomarcadores de Diagnóstico e Monitoração, Centro de Pesquisas René Rachou, Fundação Oswaldo Cruz, Belo Horizonte, MG, Brazil; Helton C. Santiago, Departamento de Bioquímica e Imunologia, Universidade Federal de Minas Gerais, Belo Horizonte, MG, Brazil.

Supplemental material for this article may be found at http://dx.doi.org/10.1128/IAI.01497-15.

ster mice (Taconic Farms) every 21 days. Animals were infected intraperitoneally with 1,000 blood-stage trypomastigote forms of *T. cruzi*. Parasitemia levels in an unstained 5-μl drop of whole blood drawn from the tail vein were determined by light microscopy at a magnification of ×400, as described previously (16). Animals were weighed weekly and monitored for clinical signs of disease. Measurements of serum creatine kinase (CK), blood urea nitrogen (BUN), alanine aminotransferase (ALT), aspartate transaminase (AST), alkaline phosphatase (ALP), lactate dehydrogenase (LDH), and amylase levels were conducted at the NIH Clinical Chemistry Laboratory.

Ethics statement. The NIAID Animal Care and Use Committee reviewed and approved this study. The protocol adhered to the U.S. Government principles and applicable humane and ethical policies as specified in the NIH policy manual, in accordance with the U.S. Public Health Service Policy on Humane Care and Use of Laboratory Animals, the Animal Welfare Act Regulations, and the National Research Council's *Guide for the Care and Use of Laboratory Animals*. This policy complies with the provisions of NIH's intramural institutional assurance (A4149-01) on file with the Office of Laboratory Animal Welfare (OLAW).

Histopathological analysis. Mouse organs were removed, washed in sterile phosphate-buffered saline (PBS), fixed in 10% buffered paraformaldehyde, and embedded in paraffin. Six-micrometer-thick sections were stained with hematoxylin and eosin (H&E) to investigate inflammation and parasitism or with Gomori's trichrome to assess collagen content. For scoring purposes, the slides were analyzed by a board-certified veterinary pathologist. A score of severity was created based on the percentage of blood vessels affected by vasculitis in the different organs analyzed. The scoring system was as follows: 0, no blood vessels affected; 1, 1 to 30% of blood vessels affected; 2, 31 to 60% of blood vessels affected; and 3, 61 to 100% of blood vessels affected.

Immunohistochemistry (IHC). Serial cryostat sections were placed on poly-L-lysine-coated glass slides and fixed for 10 min in cold acetone. The slides were then incubated in PBS containing 1% bovine serum albumin (BSA; Sigma-Aldrich, Atlanta, GA), 0.1% sodium azide, and normal goat serum (diluted 1/50) for 20 min. The following primary rat monoclonal antibodies (MAbs) were then added: anti-mouse CD8 (53-6.7) and anti-mouse CD4 (GK1.5), both from Abcam (Cambridge, MA); and anti-mouse F4/80 (BM8), anti-human/mouse CD45R/B220 (RA3-6B2), and anti-mouse Ly6G/Gr-1 (RB6-8C5), from eBioscience (San Diego, CA). A normal rat IgG2a isotype control antibody (eBR2a; eBioscience), diluted 1:20 in PBS containing 1% BSA, was used as a control. Slides were incubated for 45 min at room temperature and washed twice with PBS containing Tween (PBST), and then the secondary polyclonal biotinylated anti-rat IgG antibody (eBioscience) was added at a 1:100 dilution. The slides were incubated for 30 min at room temperature, and following a PBS wash, immunoreactivity was detected using a streptavidin-horseradish peroxidase system at a 1:400 dilution (Dako, Carpinteria, CA) after 30 min of incubation at room temperature. Color was developed with 3-amino-9-ethylcarbazole (AEC) and hydrogen peroxide (AEC substrate kit; BD Biosciences, CA), and slides were subsequently counterstained with hematoxylin, dehydrated in graded ethanol, and mounted with Dako Faramount aqueous mounting medium (Dako). Spleen sections were used as a positive control for each staining step.

Immunofluorescence microscopy. Tissue cryosections were placed on poly-L-lysine-coated glass slides, fixed in acetone for 2 min, and then washed with Tris-buffered saline containing 0.05% Triton X-100 (TBST). The slides were then incubated in 3% goat serum in TBST for 30 min to block nonspecific protein binding. Rat monoclonal anti-CD31 (1:200; BD Pharmingen, San Jose, CA) and rabbit polyclonal anti-smooth muscle cell actin (anti-SMA) (1:200; Abcam) were then applied to the slides, which were incubated for 2 h at room temperature and then washed three times with TBST. Goat polyclonal anti-rat IgG antibody conjugated to Alexa Fluor 488 (1:2,000; Jackson ImmunoResearch, West Grove, PA) and goat polyclonal anti-rabbit IgG antibody conjugated to Alexa Fluor 594 (1:2,000; Life Technologies, Carlsbad, CA) were added. The slides were incubated for 1.5 h at room temperature and then, following TBST washing, counterstained with DAPI (4′,6-diamidino-2-phenylindole; Life Technologies), washed with TBST, and mounted with Prolong Gold (Life Technologies). Confocal microscopy imaging was performed with a Leica SP5 microscope (Buffalo Grove, IL), a UV laser source for DAPI fluorescence, an argon laser source for Alexa Fluor 488 fluorescence, and a tunable white-light laser (WLL) for Alexa Fluor 594 fluorescence. Sera from three chronically *T. cruzi*-infected mice (10 months postinfection [p.i.]) and one uninfected mouse were collected separately and used for parasite detection in tissues as detailed below. Formalin-fixed and paraffin-embedded tissue sections were deparaffinized and rehydrated in increasing dilutions of ethanol and then washed with TBST. The slides were then incubated in 3% goat serum and 0.2% fish gelatin (Sigma-Aldrich) in TBST for 1 h to block nonspecific protein binding. Serum from each mouse was diluted 1:30 in 0.2% fish gelatin in TBST, applied to the deparaffinized sections at room temperature for 2 h, and then washed three times with TBST. Goat polyclonal anti-mouse IgG antibody conjugated to Alexa Fluor 594 (1:2,000; Life Technologies) was added. The slides were incubated for 1.5 h at room temperature and then, following TBST washing, counterstained with DAPI (Life Technologies), washed with TBST, and mounted with Prolong Gold (Life Technologies).

mRNA analysis. Real-time reverse transcription-PCR (RT-PCR) was performed as previously described (17), with minor modifications, using tissues from infected and control mice. Total RNA was isolated using an RNeasy kit (Qiagen, Valencia, CA), and real-time RT-PCR was performed on an ABI Prism 7900 sequence detection system (Applied Biosystems, Foster City, CA), using SYBR green PCR master mix (Applied Biosystems), after reverse transcription of 1 μg RNA with Moloney murine leukemia virus (M-MLV) reverse transcriptase (Promega, Madison, WI). The relative level of gene expression was determined by the comparative threshold cycle method as described by the manufacturer, with data for each sample normalized to hypoxanthine phosphoribosyltransferase (HPRT) and expressed as the fold change compared with uninfected controls. The primer sequences are available upon request.

Quantification of parasite tissue loads by real-time PCR. Real-time PCR was performed as described previously (17). Briefly, on different days after infection, DNA was extracted from the heart, spleen, and liver by use of a DNeasy kit (Qiagen). Real-time PCR using 50 ng of total DNA was performed on an ABI Prism 7900 sequence detection system, using SYBR green PCR master mix according to the manufacturer's recommendations. The level of host DNA was determined by measurement of genomic interleukin-12 (IL-12) p40 PCR product levels in the same samples. Purified *T. cruzi* DNA, obtained from trypomastigote cultures maintained *in vitro*, was sequentially diluted for standard curve generation in an aqueous solution containing equivalent amounts of DNA from uninfected mouse tissues. The following *T. cruzi*-specific primers were used, targeting a 195-bp repeat in the *T. cruzi* satellite sequence: 5′-GCTCTTGCCCACA MGGGTGC-3′ (forward), where M = A or C, and 5′-CCAAGCAGCGG ATAGTTCAGG-3′ (reverse). The genomic IL-12 p40-specific primers were 5′-GTAGAGGTGGACTGGACTCC-3′ (forward) and 5′-CAGATG TGAGTGGCTCAGAG-3′ (reverse).

Ultrasound measurement. The ejection fraction was measured by ultrasound at the NIH Clinical Center Mouse Imaging Facility (MIF/NIH). Animals were anesthetized with isoflurane. An Acuson Sequoia (8 to 15 MHz) or Visualsonics (30 to 55 MHz) ultrasound machine was used. The transducer was used for parasternal short- and long-axis views. Imaging was produced with the aid of warmed coupling gel. Mice were kept warm on a pad with circulating warm water and by use of a radiant heat lamp. The echo took about 15 to 30 min, and B-mode, M-mode, and Doppler images were acquired. Mice recovered in a warmed recovery cage/box.

ELISA. Serum antibodies against *T. cruzi* were quantified by enzyme-linked immunosorbent assay (ELISA). In brief, 96-well flat-bottom ELISA plates were coated with *T. cruzi* antigen (0.5 μg/ml) for 2 h at room temperature. Plates were blocked with 0.5% gelatin for 1 h at 37°C. After

washing, 100-μl aliquots of mouse plasma samples, diluted 1:200 in PBS, were added, and the plates were incubated at 37°C for 2 h. After washing, goat anti-mouse IgG and IgM antibodies, diluted 1:2,500 and 1:1,000, respectively, in PBST, were added and incubated at 37°C for 2 h. The plates were then washed and developed using secondary antibodies labeled with alkaline phosphatase, diluted to 1:2,500 in PBST. The BluePhos AP substrate was added to produce color, and the absorbance was measured at 630 nm by using a microplate reader (Spectra Max M5; Molecular Devices, Sunnyvale, CA). All antibodies, including conjugates, were obtained from KPL (Gaithersburg, MD).

Flow cytometry. Flow cytometry was performed as previously described (17), with modifications. Briefly, animals were first euthanized under CO_2 anesthesia. Popliteal lymph nodes were pooled and dissociated by passing tissue through a 70-μm nylon cell strainer in RPMI 1640 (Invitrogen, Carlsbad, CA) containing 10% fetal bovine serum (FBS). Spleens and skeletal muscle from hind limbs were removed and placed in serum-free RPMI 1640 (Invitrogen, Carlsbad, CA). They were minced and incubated with Liberase TL (2 mg/ml; Roche Applied Sciences, Indianapolis, IN) and DNase I (100 mg; Sigma-Aldrich) for 30 min. Single-cell suspensions were prepared by passing tissue through a 100-μm nylon cell strainer in PBS containing 2% FBS (HyClone, Thermo Scientific, Waltham, MA) and EDTA. The cell suspension from skeletal muscle was centrifuged in 35% Percoll (Amersham-Pharmacia Biotech, Piscataway, NJ) for 15 min at 700 × *g*. Spleen and skeletal muscle suspensions were hemolyzed in ACK buffer (Lonza BioWhittaker, Walkersville, MD). A total of 10^6 freshly isolated cells were analyzed immediately *ex vivo* for surface marker expression or after being cultured for 18 h or 6 h with *T. cruzi* antigen or with phorbol myristate acetate (PMA) (50 ng/ml) and ionomycin (500 ng/ml), respectively, for intracellular cytokine expression. Cells were also cultured with medium alone for basal intracellular cytokine expression. During the last 4 h of culture, brefeldin A and monensin (1 mg/ml [each]) (BD Pharmingen, San Jose, CA) were added for intracellular cytokine staining. Before adding antibodies, cells were washed in PBS and incubated for 30 min with an amine-reactive fluorescent dye to exclude dead cells (LIVE/DEAD Fixable Blue dead cell stain kit; Invitrogen, Grand Island, NY). The following labeled rat or hamster anti-mouse MAbs were used: anti-CD3–Alexa Fluor 700 (17A2), anti-CD8–allophycocyanin–Alexa Fluor 750 (53-6.7), anti-Ly6G–eFluor 450 (RB6-8C5), anti-F4/80–phycoerythrin (PE)–Cy5 (BM8), anti-B220–peridinin chlorophyll protein (PerCP)–Cy5.5 (RA3-6B2), anti-Ly6C–PE–Cy7 (HK1.4), anti-CD11c–PE (N418), anti-NK1.1–fluorescein isothiocyanate (FITC) (PK136), and anti-CD11b–allophycocyanin (M1/70), all from eBioscience (San Diego, CA); anti-I-A/I-E–biotin (2G9), from BD Pharmingen (San Jose, CA); and anti-CD4–Pacific orange (RM4-5), from Caltag-Invitrogen (Carlsbad, CA). Cell suspensions were then fixed and permeabilized according to the manufacturer's instructions (Fix/Perm kit; BD Pharmingen). To analyze activation markers, the cell suspensions were stained with the following labeled rat anti-mouse MAbs: anti-CD44–Pacific blue (IM7), from BioLegend (San Diego, CA); and anti-CD62L–PE–Cy7 (MEL-14), from eBioscience (San Diego, CA). Intracellular staining was performed using the following labeled rat or hamster anti-mouse MAbs: anti-IL-17A–PerCP–Cy5.5 (TC11-18H10), from BD Pharmingen; and anti-gamma interferon (anti-IFN-γ)–PE–Cy7 (XMG1.2) and anti-tumor necrosis factor alpha (anti-TNF-α)–Pacific blue (MP6-XT22), from eBioscience. Quantum dot 605-conjugated streptavidin (Invitrogen, Carlsbad, CA) was added during intracellular staining to bind anti-I-A/I-E–biotin. Data were collected using an LSR II flow cytometer (BD Immunocytometry Systems) with Diva software (BD Biosciences) and were analyzed with FlowJo software (Tree Star, Ashland, OR).

MHC-I peptide tetramer staining. Major histocompatibility complex class I (MHC-I) tetramers were synthesized at the NIH Tetramer Core Facility (Emory University, Atlanta, GA). The tetramer used in this study was TSKB20 (ANYKFTLV/Kb), and the protocol used has been described previously (18) but was performed with some modifications. Briefly, single-cell suspensions of the spleen, popliteal lymph nodes, or skeletal muscle were cultured for 18 h with either medium alone or *T. cruzi* antigen (25 mg/ml). Before adding antibodies, cells were washed in PBS and incubated for 30 min with an amine-reactive fluorescent dye to exclude dead cells (LIVE/DEAD Fixable Violet dead cell stain kit; Invitrogen). Cells were then washed in PBS-0.5% bovine serum and stained for 30 min at room temperature with TSKB20/Kb-phycoerythrin (5 mg/ml). After this step, we proceeded as described above for intracellular cytokine staining. For the analysis, at least 200,000 events in the mononuclear gate (forward scatter [FSC] versus side scatter [SSC]) were acquired.

Statistical analyses. Results are shown as means ± standard errors of the means (SEM). Differences between groups were compared using the Mann-Whitney test (two sets of data) or one-way analysis of variance (ANOVA) (three or more sets of data), followed by the Student-Newman-Keuls *post hoc* test. Survival curves were analyzed using the log rank test. Differences were considered significant if the P values were <0.05.

RESULTS

Mice infected with *T. cruzi* clear acute parasitemia but then develop hind limb paralysis late after infection. C57BL/6J mice infected intraperitoneally with the myotropic Colombiana strain of *T. cruzi* were monitored for development of clinical signs of disease, with the goal of studying a model of chronic chagasic cardiomyopathy. As expected, all mice developed high-level parasitemia, which was cleared by day 90 p.i. (data not shown), confirming previously published results for the model (17). The mice then appeared to be healthy until approximately 5 months p.i., when muscle atrophy of the hind limbs and difficulty ambulating were first observed in some mice. By 8 to 12 months p.i., ~75% of infected animals exhibited hind limb paresis or frank paralysis (Fig. 1A), whereas uninfected age-matched control mice all remained fully ambulatory, without any signs of weakness ($P = 0.0003$; log rank test). By 15 months p.i., when the experiment was terminated, mortality in the infected group was 30%, whereas all uninfected mice survived (Fig. 1B); however, this difference was not statistically significant (log rank test).

Mice develop vasculitis in multiple organs late after *T. cruzi* infection. Histopathological analysis of skeletal muscle from the hind limbs of mice (quadriceps femoris and gastrocnemius) presenting with clinical signs of weakness and paralytic disease (7 to 12 months p.i.) showed prominent arteritis characterized by fibrinoid necrosis and nonsuppurative inflammation of the intima and adventitia. The muscle itself showed myofiber atrophy, fibrosis, and nonsuppurative inflammation, with replacement by adipose tissue (Fig. 1C). The vascular lesions varied in size and predominantly affected arteries and arterioles.

Quantitative analysis revealed that almost 100% of infected mice studied between 7 and 15 months p.i. had vascular lesions in skeletal muscle (Fig. 1D). Both male and female mice were affected similarly (see Fig. S1A in the supplemental material). Grossly normal muscle from the head had vasculitis, but inflammation, atrophy, and fatty replacement were much less severe. For example, 100% of animals analyzed had lesion severity scores of 2 or 3 for the masseter, temporalis, and ventral muscles of the jaw, but this did not overtly affect the feeding behavior of the mice or their weight (see Fig. S1B). In contrast, no signs of inflammation surrounding blood vessels or myofibers were found in skeletal muscle of uninfected age-matched control mice (Fig. 1C).

Arteritis was not restricted to skeletal muscle in infected mice but was also present, to a lesser extent, in the skin, nerves, bladder, intestine, myocardium, and pancreas (Fig. 1D and E; see Fig. S2A

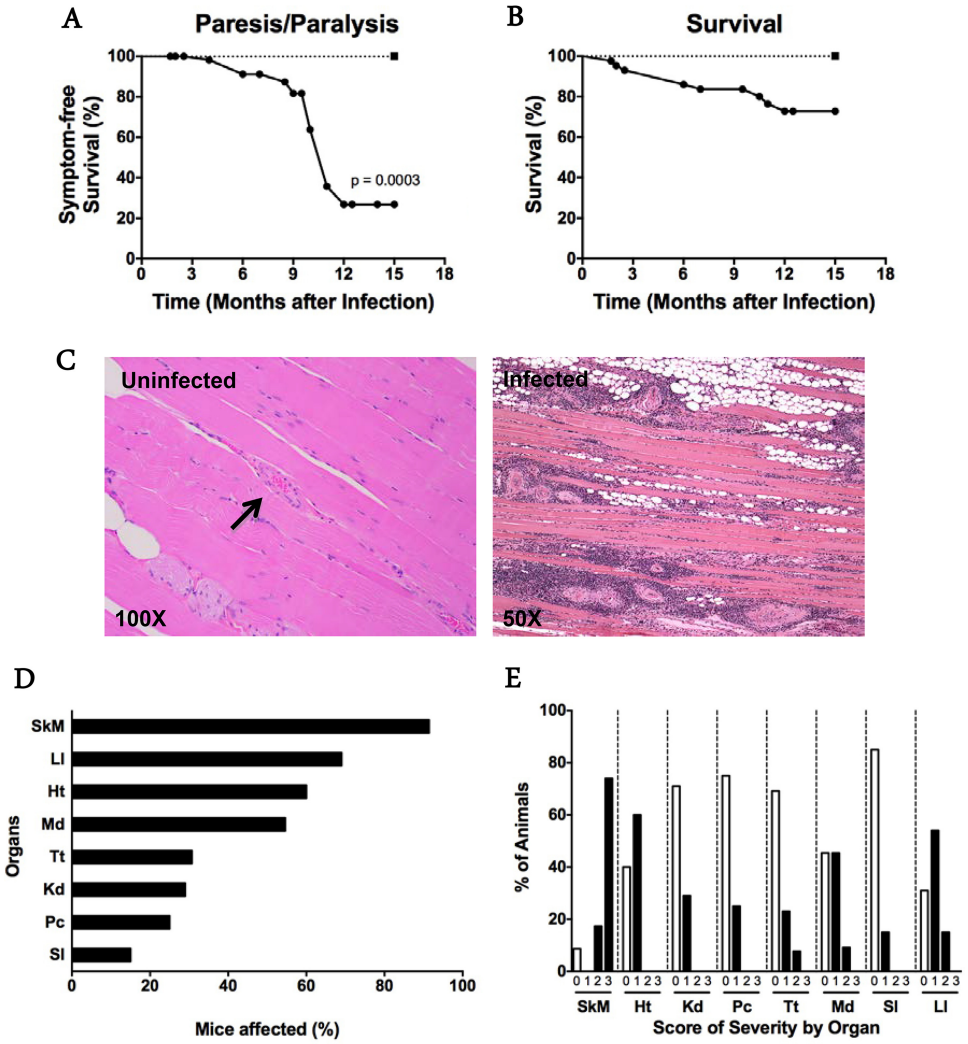

FIG 1 *T. cruzi* causes systemic arteritis late after infection in C57BL/6J mice. (A and B) Paresis/paralysis and survival were monitored over time. Paresis/paralysis refers to the posterior limbs. For panels A and B, 60 and 43 infected mice, respectively (closed circles), and 10 uninfected age-matched control mice (closed squares) were monitored. For panel A, $P = 0.0003$; for panel B, the curves are not statistically significantly different (log rank test). (C) Representative H&E-stained sections of quadriceps muscles from a chronically infected mouse and an age-matched uninfected control. Arrow, normal arteriole. Images are representative of groups of 12 infected and 8 uninfected mice tested at 7 to 12 months p.i. The prevalence (D) and severity (E) of vasculopathy in mouse organs are indicated by graphs. The severity scoring system was based on the percentage of vessels with lesions, as follows: 0, no lesions; 1, 1 to 30%; 2, 31 to 60%; and 3, 61 to 100%. Abbreviations: Pc, pancreas; Ht, heart; Kd, kidney; LI, large intestine; Md, mediastinum; SI, small intestine; SkM, skeletal muscle; Tt, testis. Data were pooled from two independent experiments, with a total of 11 to 25 animals, at 7 to 15 months p.i.

in the supplemental material). On the other hand, some organs were not affected, including the brain, liver, lungs, esophagus, and spleen (see Fig. S2B). The rank order of affected organs, determined by the percentage of mice with arteritis in a particular organ, was as follows: skeletal muscle ≫ large intestine > testis > heart > kidney > pancreas > small intestine (Fig. 1D; see Fig. S2A; also data not shown). A pathological severity scoring system was created to measure the percentage of blood vessels affected in each organ analyzed. Again, skeletal muscle was the most severely affected tissue, with ~75% of mice having 61 to 100% of arteries affected (Fig. 1E). In other tissues, such as the testis and large intestine, 31 to 60% of blood vessels were affected, but in fewer than 20% of mice analyzed. Interestingly, although chronic arteritis was present in the heart in 60% of mice, only 1 to 30% of arteries scored were affected, despite the fact that the degrees of inflammation in heart and skeletal muscle were similar during acute infection (data not shown). Chronically infected animals had no significant defects in hematocrit or total or differential white blood cell count (data not shown).

We next investigated the histopathologic development of skeletal muscle arteritis as a function of time after *T. cruzi* infection (Fig. 2A). Two months after infection, inflammatory infiltrates were concentrated around small to medium-sized arteries but were also dispersed between myocytes. At 4 months, inflammation was more selectively perivascular in distribution. This was more evident at 7 months. By 10 months, vasculitis was even more intense in skeletal muscle and was associated with myofiber loss and fatty replacement. The full spectrum of lesion severity could be observed in the same muscle from the same animal even 11 months after infection (data not shown). During this progression,

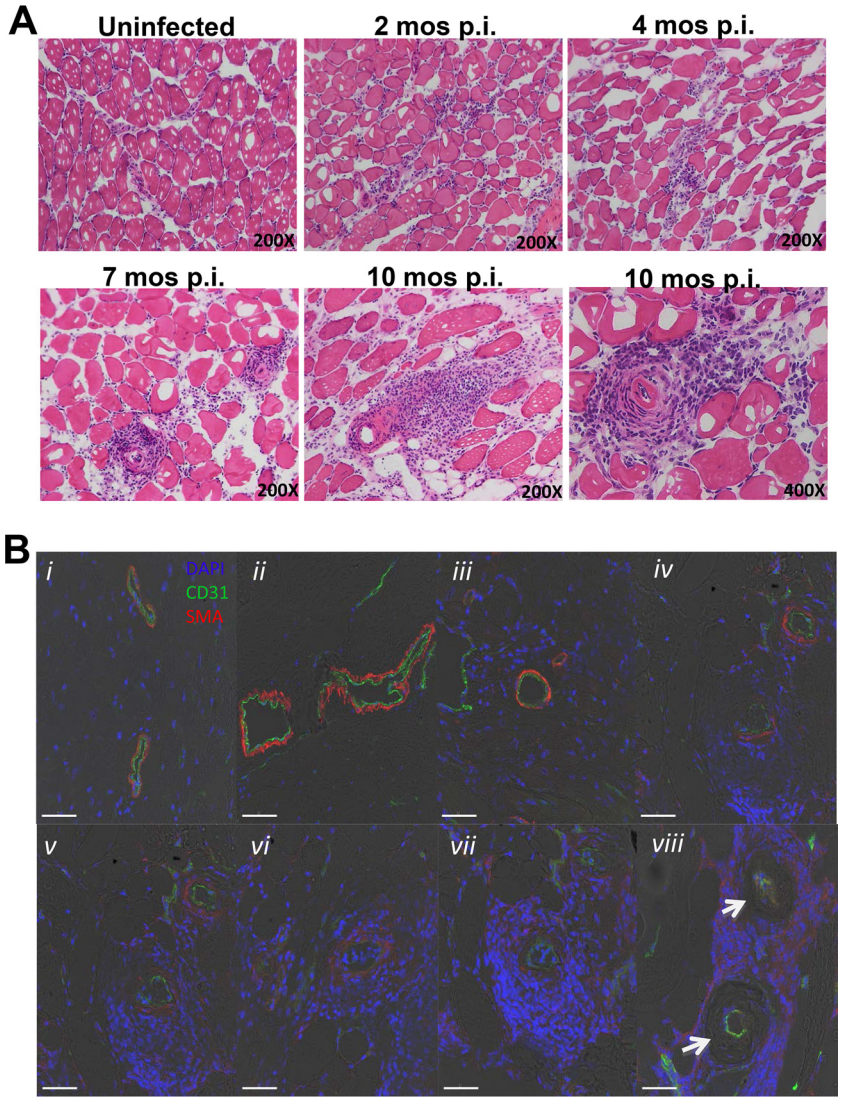

FIG 2 Histopathology of systemic necrotizing vasculitis lesions in skeletal muscle late after *T. cruzi* infection of C57BL/6J mice. Sections of quadriceps muscles were analyzed. (A) Time course of infection. Samples were obtained from mice at the indicated time points after infection and stained with H&E. Images are representative of a total of 3 mice analyzed per time point. (B) Development of fibrinoid necrosis. Samples of vascular lesions with different degrees of severity (i to viii) were stained for immunofluorescence with DAPI (blue) and with antibodies directed against CD31 (green) and smooth muscle cell actin (SMA) (red). Images are representative of 3 mice analyzed 10 months after infection. Confocal immunofluorescence images are superimposed on bright-field images. Arrows, absence of smooth muscle actin.

endothelium, as defined histologically by staining for the marker CD31, remained intact, whereas staining of smooth muscle cell actin (SMA) eventually completely disappeared, consistent with loss of the tunica media through fibrinoid necrosis (Fig. 2B). We did not see fibrosis in the vascular lesions in this model.

By immunohistochemistry, we found a mixed cellular infiltrate that included mostly $CD8^+$ T cells and $F4/80^+$ myeloid cells (probably monocytes and macrophages) (Fig. 3). Staining with the anti-neutrophil antibody 7/4 revealed relatively weak immunoreactivity in the lesions (see Fig. S3 in the supplemental material). Consistent with the presence of inflammatory macrophages, immunoreactivity for inducible nitric oxide synthase (iNOS) was detectable in the lesions (Fig. 3). The lesions did not stain positively for B lymphocytes (B220) (data not shown). Together, these features are consistent with a pathological diagnosis of systemic necrotizing vasculitis.

Pathogen-specific type I immune responses in skeletal muscle in mice chronically infected with *T. cruzi*. For a more comprehensive phenotypic and functional characterization of the cells present in the lesions, we performed enzymatic digestion of the quadriceps muscle to isolate leukocytes for flow cytometry. We confirmed that most of the cells found in muscles from infected mice were $CD3^+$ lymphocytes ($158.6 \times 10^5 \pm 55.3 \times 10^5$ cells) and antigen-presenting cells (APCs) ($81.4 \times 10^5 \pm 26.4 \times 10^5$ cells) (Fig. 4). Neutrophils were not detectable, suggesting either that they were dead, and thus gated out, or that the low level of MAb 7/4 immunoreactivity detected by IHC was due to macrophage staining. Most of the APC population was comprised of inflammatory monocytes ($CD3^-$ $CD11c^-$ $Ly6G^-$ $Ly6C^+$) ($51.4 \times 10^5 \pm 22.2 \times 10^5$ cells) or monocytes/macrophages ($CD3^-$ $CD11c^-$ $Ly6G^-$ $Ly6C^-$ $F4/80^+$) ($29.6 \times 10^5 \pm 10 \times 10^5$ cells) (Fig. 4B, lower graph). Most of the $CD3^+$ T cell population

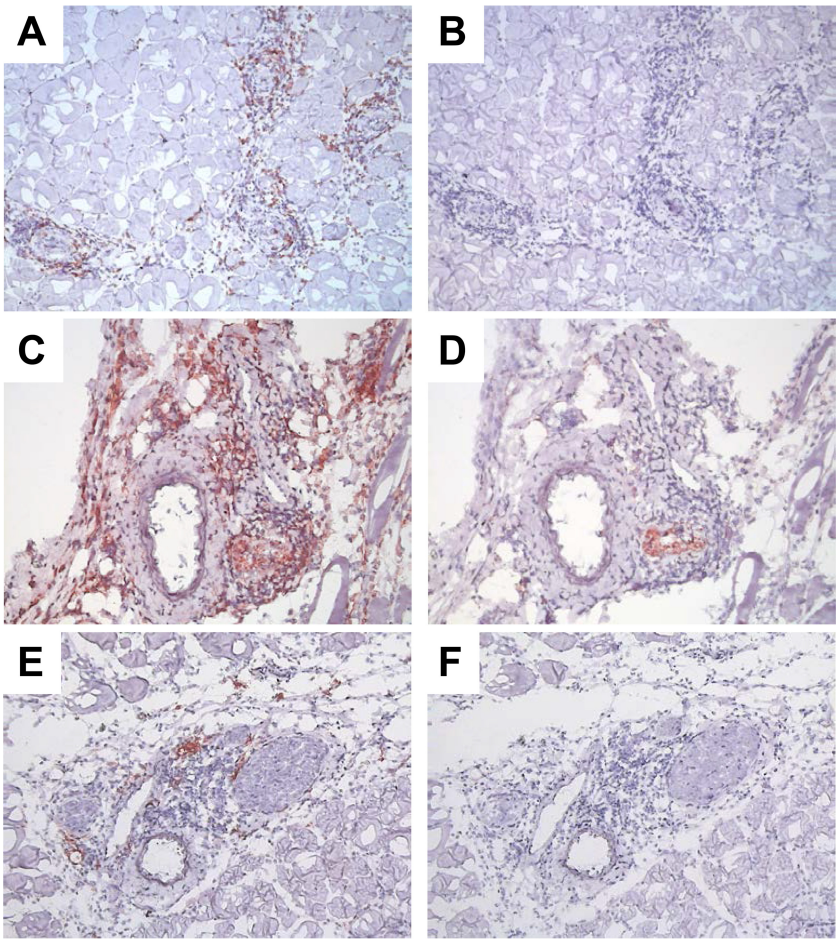

FIG 3 Distribution of T lymphocytes and macrophages in systemic necrotizing vasculitis lesions in skeletal muscles from *T. cruzi*-infected mice. Serial sections of skeletal muscle from posterior limbs of 7-month-infected mice were stained with specific antibodies for CD8 (A), F4/80 (B), and iNOS (C) or the respective isotype control antibodies (B, D, and F, respectively) and counterstained with Mayer's hematoxylin. Images are representative of 3 infected mice that were analyzed. Magnification, ×150 (A, B, E, and F) or ×200 (C and D).

was $CD8^+$ ($951.4 \times 10^4 \pm 398 \times 10^4$ $CD8^+$ cells versus $549 \times 10^4 \pm 147.7 \times 10^4$ $CD4^+$ cells; $P = 0.03$) (Fig. 4B, middle graph), and the great majority of both $CD8^+$ and $CD4^+$ T cell subpopulations was activated ($CD62L^-$ $CD44^{hi}$) (for $CD8^+$ cells, $527 \times 10^4 \pm 229 \times 10^4$ activated cells versus $22.6 \times 10^4 \pm 9.2 \times 10^4$ naive cells [$P = 0.0006$]; and for $CD4^+$ cells, $383.1 \times 10^4 \pm 121.6 \times 10^4$ activated cells versus $8.4 \times 10^4 \pm 4.5 \times 10^4$ naive cells [$P = 0.0006$]) (Fig. 5A and B). We found that the $CD4^+$ T cells detectable by fluorescence-activated cell sorting (FACS) were distributed mainly around the skeletal muscle myocytes and were not associated with the arterial lesions (data not shown). After *in vitro* restimulation with PMA and ionomycin, the majority of $CD4^+$ and $CD8^+$ cells extracted from skeletal muscle were found to be IFN-γ^+. Many of these were double producers of both IFN-γ and TNF-α ($453.9 \times 10^3 \pm 294 \times 10^3$ $CD4^+$ IFN-γ^+ TNF-α^+ cells and $670.7 \times 10^3 \pm 312.3 \times 10^3$ $CD8^+$ IFN-γ^+ TNF-α^+ cells) (Fig. 5C). Few $CD4^+$ or $CD8^+$ cells were singly positive for IL-17A (data not shown), and no $CD8^+$ cells were found to be doubly positive for IFN-γ and IL-17A (Fig. 5C).

In an attempt to identify a *T. cruzi*-specific population of $CD8^+$ T lymphocytes, we used the tetramer TSKB20 (peptide ANYKFTLV), which was previously characterized and reported to be an immunodominant peptide for *T. cruzi* infection of C57BL/6 mice (18). Isolated cells were restimulated *in vitro* in the presence of *T. cruzi* antigen or PMA-ionomycin and stained with TSKB20 tetramer and monoclonal antibodies for cytokines. Approximately 15% of the total $CD8^+$ population isolated from skeletal muscles of infected mice was found to be $TSKB20^+$ after specific stimulation (Fig. 5E). Moreover, after mitogenic stimulation, approximately 60% of tetramer-specific $CD8^+$ cells were IFN-γ^+ TNF-α^-, and 35% were IFN-γ^+ TNF-α^+ (Fig. 5D and data not shown). In contrast, for cells obtained from popliteal lymph nodes and the spleen, we found that only background levels of total $CD8^+$ T cells were tetramer specific (Fig. 5E). Consistent with a type I adaptive immune response in the lesions, we observed selectively increased expression of mRNAs for the type I chemokines Cxcl10/IP-10 (19- ± 25.3-fold induction; $P = 0.0081$) and Ccl5/RANTES (277.1- ± 240.4-fold induction; $P = 0.0121$) (Fig. 6). We also detected higher expression of Ccr2 (21.8- ± 41.3-fold induction; $P = 0.0485$), a chemokine receptor for Ccl2, Ccl7, and Ccl12, which are all chemoattractants for inflammatory monocytes. The immune response to *T. cruzi* is also strongly skewed toward Th1 during acute infection (data not shown).

Localization of low levels of persistent parasites in chronically *T. cruzi*-infected mice. To test whether the immune response in skeletal muscle might be driven by local parasite persis-

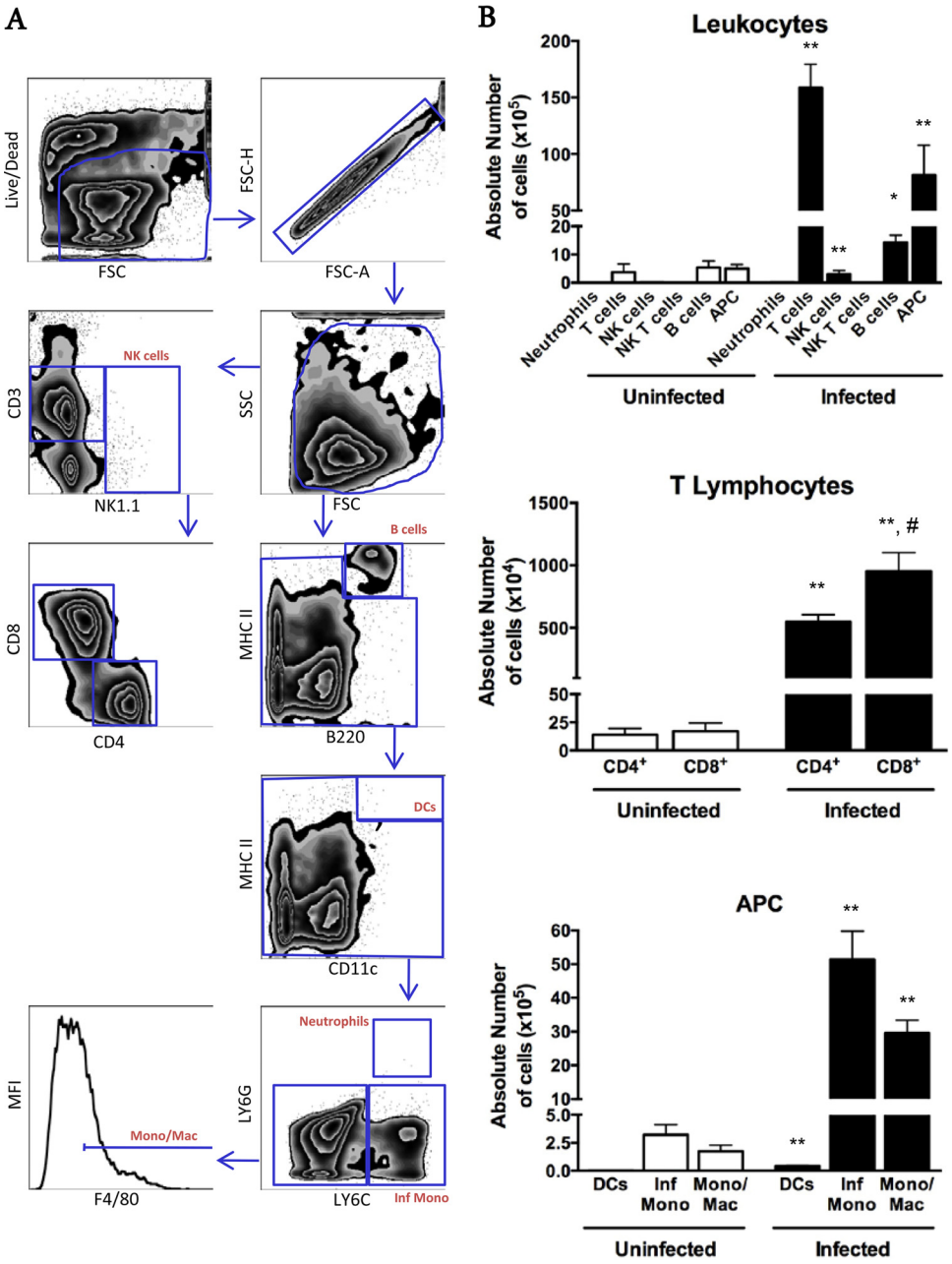

FIG 4 Flow cytometric analysis of leukocyte subsets extracted from skeletal muscles of paretic chronically *T. cruzi*-infected mice. (A) Gating strategy. (B) Quantitative data for the indicated leukocyte subsets. Black bars, infected mice; white bars, respective age-matched uninfected controls. Mono/Mac, monocytes/macrophages; Inf Mono, inflammatory monocytes; APC, antigen-presenting cells; DCs, dendritic cells. Data are from a representative experiment of a total of 2 independent experiments ($n = 7$ infected and 4 uninfected mice). *, $P < 0.05$ compared to uninfected controls; **, $P < 0.01$ compared to uninfected controls; #, $P < 0.05$ for infected $CD8^+$ versus infected $CD4^+$ T cells, according to the Mann-Whitney test.

tence, we measured parasite burdens in paretic mice late after *T. cruzi* infection. After control of acute infection, parasitemia was not detectable in *T. cruzi*-infected mice at late time points p.i. by standard light microscopy. Nevertheless, a *T. cruzi* DNA-specific PCR survey identified evidence of the parasite at the genetic level. By this measure, parasite burdens were very low in organs from chronically infected mice compared to levels in acutely infected hearts and were restricted mainly to organs in which systemic necrotizing vasculitis was observed (Fig. 7A). Consistent with this, amastigote nests (pseudocysts) were rarely detected and were seen only in organs where vasculitis was observed. In skeletal muscle, parasites appeared to be within skeletal muscle myocytes. One such nest is shown adjacent to an area of vasculitis in Fig. 7B; however, there was no consistent colocalization of parasites with arterial lesions within affected organs, and there was little inflammation immediately surrounding myocytes positive for amastigote nests.

To address the possibility that vasculitis might also or instead

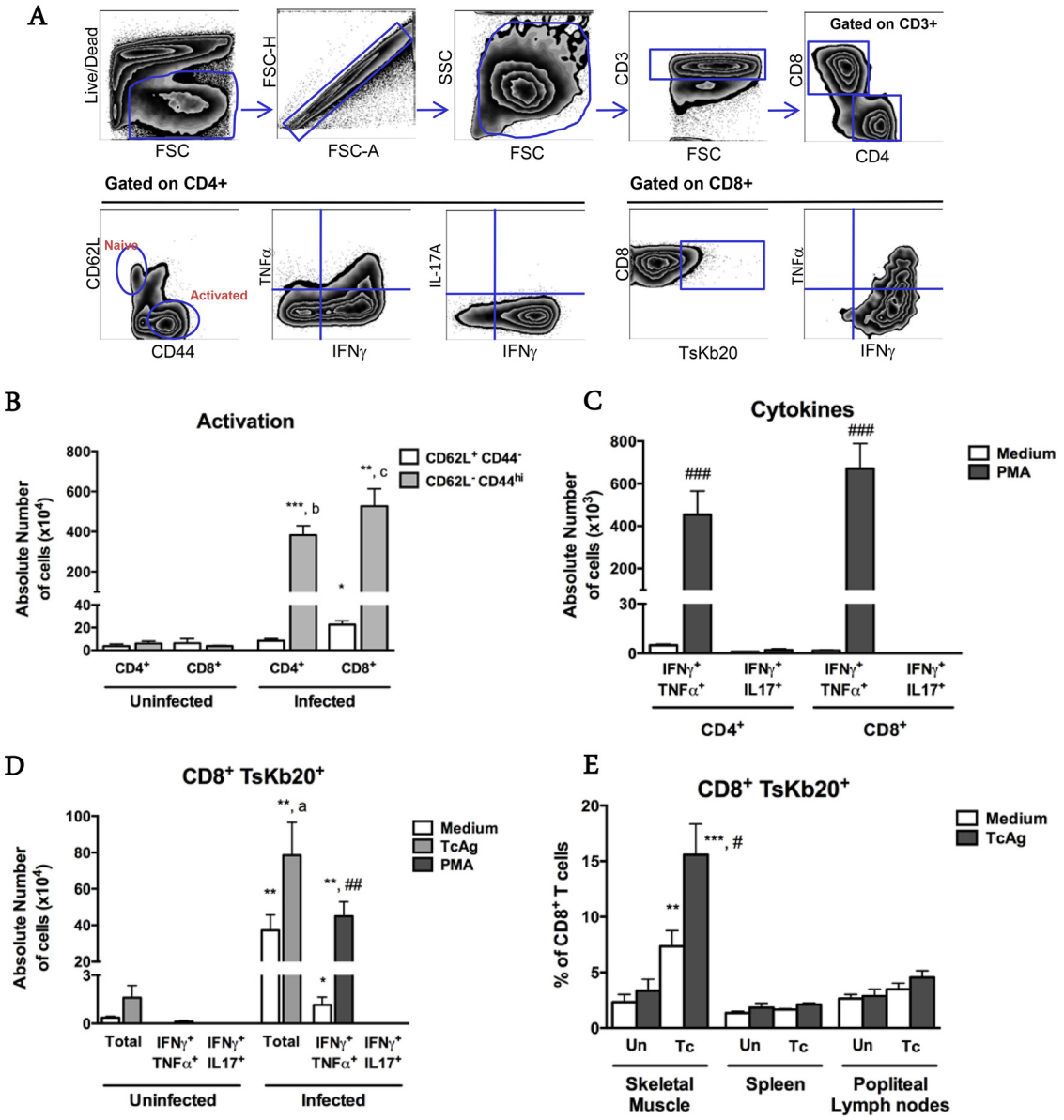

FIG 5 Local *T. cruzi*-specific type I-skewed immune responses in skeletal muscles from chronically *T. cruzi*-infected mice. (A) Gating strategy. (B to E) Quantitative data for the indicated T cell functional states, analyzed after extraction of leukocytes from the indicated tissue or organ. (B) Lymphocytes were analyzed *ex vivo*. (C) T cells were restimulated *in vitro* with PMA-ionomycin or medium for 6 h. (D and E) T cells were restimulated *in vitro* with PMA-ionomycin for 6 h or with *T. cruzi* antigen (TcAg) or medium for 18 h. In panel E, "Un" denotes uninfected mice, and "Tc" denotes *T. cruzi*-infected mice. Data are from a representative experiment of a total of 2 independent experiments ($n = 7$ infected and 4 uninfected mice). *, **, and ***, $P < 0.05$, $P < 0.01$, and $P < 0.005$, respectively, for comparing corresponding uninfected and infected subpopulations; a, $P < 0.05$ for comparing medium and TcAg-stimulated conditions; b, $P < 0.01$ for comparing $CD4^+$ subpopulations in infected mice; c, $P < 0.005$ for comparing $CD8^+$ subpopulations in infected mice; #, ##, and ###, $P < 0.05$, $P < 0.01$, and $P < 0.005$, respectively, for comparing medium- and PMA-stimulated subpopulations. Statistical analysis was performed by the Mann-Whitney test.

be driven by a pathogen-initiated autoimmune response, we examined antibodies produced by chronically infected mice. As shown in Fig. 8A, *T. cruzi*-infected mice had high titers of specific IgM (average optical density [OD] for infected mice, 0.88; and that for uninfected mice, 0.02) and IgG (average OD for infected mice, 1.1; and that for uninfected mice, 0.007) during chronic infection (300 days after infection). Immunofluorescence microscopy revealed that sera from chronically *T. cruzi*-infected mice were able to specifically stain parasites *in situ* in skeletal muscles from chronically infected mice, confirming the histopathologic data presented in Fig. 7B. Sera from uninfected mice were nonreactive with tissue from infected mice. Again, parasites revealed by this technique appeared to all be in an intracellular location and were not clearly colocalized with vasculitis. No other specific staining was revealed by the sera from *T. cruzi*-infected mice, and the anti-mouse secondary antibody did not reveal antibody deposits in the arterial lesions (Fig. 8B and C). The parasite-infected cell shown in Fig. 8C appears to be surrounded by inflammatory cells.

To investigate the functional effects of vasculitis in infected

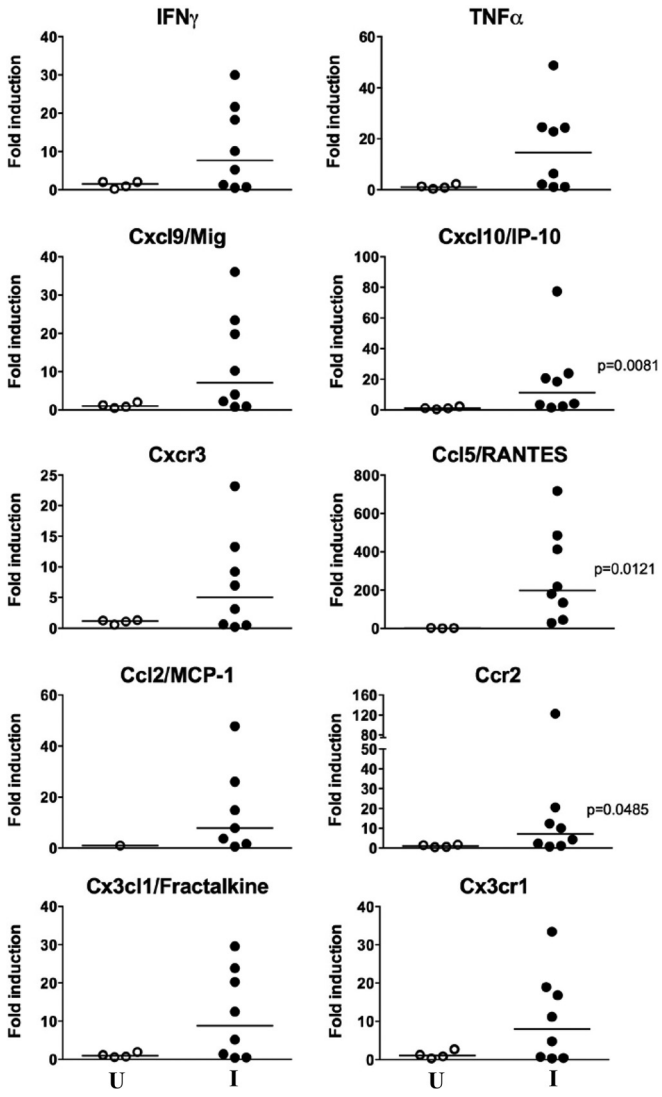

FIG 6 Development of a type I-skewed immune environment in skeletal muscles from chronically *T. cruzi*-infected mice. Mice were euthanized after developing atrophy and/or partial or total paralysis of the posterior limbs (10 to 12 months p.i.). Expression of mRNAs for the indicated factors was determined by real-time RT-PCR. Filled circles, infected mice (I); open circles, age-matched uninfected controls (U). Data are from one experiment and are presented as individual values and medians. Statistical analysis was performed by the Mann-Whitney test.

mice beyond the association with hind limb weakness and paralysis, we performed a survey of biochemical markers of liver, kidney, pancreas, and muscle damage (see Fig. S4 in the supplemental material). Only LDH was elevated in paretic mice late after *T. cruzi* infection (511.1 ± 120.6 units/liter of blood for infected mice versus 253.3 ± 48.4 units/liter of blood for uninfected mice; $P < 0.0001$). Of particular interest, CK levels were normal, suggesting that skeletal muscle atrophy and weakness were not driven mainly or solely by ongoing muscle necrosis; levels of AST, another skeletal muscle marker, were also normal. Since cardiac disease is usually the main manifestation of Chagas' disease, we also investigated the myocardial function of mice late after *T. cruzi* infection when vasculitis had developed. Fibrosis was present in the hearts of infected mice, as evidenced by enhanced staining of collagen by Gomori's trichrome, in contrast to those of uninfected age-matched control mice (Fig. 9A and B). The staining was observed surrounding blood vessels and inflammatory infiltrates. A more intense pattern of staining was found in hearts from mice with left ventricle dilatation by ultrasound, suggesting that the cardiac disease observed in these mice may have been related to fibrosis, as it is in Chagas' disease patients. A reduced ejection fraction, a sign of cardiac failure, was observed in ~33% of mice (9 of 27 animals) by ultrasound at 7 months p.i. (average of 39% for infected mice versus 46% for uninfected mice; $P = 0.0394$ according to Fisher's exact test; odds ratios were not different) (Fig. 9C). Myocarditis was also evident in chronically *T. cruzi*-infected hearts.

DISCUSSION

In the present study, we show that a specific infectious protozoan, *T. cruzi*, can cause chronic systemic necrotizing vasculitis in mice. Our results are consistent with older reports of arteritis in skeletal muscle, skin, nerve, heart, and other tissues associated with adventitial infiltration by lymphocytes and macrophages in chronically *T. cruzi*-infected mice (3–10, 19), as well as skeletal muscle vasculitis in *T. cruzi*-infected humans (20). We extend these earlier studies by providing the first detailed description of the cellular and humoral immune responses in the lesions. Together, our findings add support to the notion that an infectious agent may cause vasculitis and provide a model for defining the parasite-driven immunopathogenesis of vasculitis.

The spectrum of vasculitis in humans is broad, and subtype classification depends on the types of blood vessels and organs involved, the nature of the inflammatory infiltrate, and the presence of necrosis, granulomas, and anti-neutrophil cytoplasmic antibodies (ANCA), among other factors. The vascular pathology in chronically *T. cruzi*-infected mice has some features that resemble human polyarteritis nodosa (PAN) with regard to multiorgan involvement of medium-sized to small arteries (21), fibrinoid necrosis, mixed cellular infiltrates including pathogen-specific $CD8^+$ T cells and macrophages (22), lack of immune complex deposition in lesions, and involvement of muscles, skin, and nerves (23–26). The most notable and interesting differences between the mouse vasculitis we analyzed and PAN include an absence in the mouse of the eponymous skin vasculitic nodules found in human PAN, a lack of neutrophilic inflammation in the mouse, and the relative prominence of the extreme involvement of skeletal muscle in the mouse, which is associated with muscle weakness and paralysis. The exact cause of weakness in mice is not known, but it may include ischemia due to skeletal muscle vasculitis, neurogenic ischemia due to vascular lesions affecting the blood supply to adjacent peripheral nerves, or both. Myositis may also contribute, although this is unlikely to be the sole or main cause, since the severity is mild and the serum muscle enzyme levels in blood are not elevated.

Our data are consistent with the notion that a massive, strongly type I-skewed and parasite-specific cellular immune response succeeds in suppressing the parasite to very low levels but fails to achieve sterile immunity, as the parasite succeeds in eluding the immune system within rare intracellular amastigote nests. The high frequency of $CD8^+$ T cells in the lesions that are specific for a single parasite antigen suggests that most, if not all, of the $CD8^+$ T cells in the lesions are parasite specific. Together with the absence of immune complexes in the lesions, the evidence supports parasite-specific cellular immune responses, not parasite-induced au-

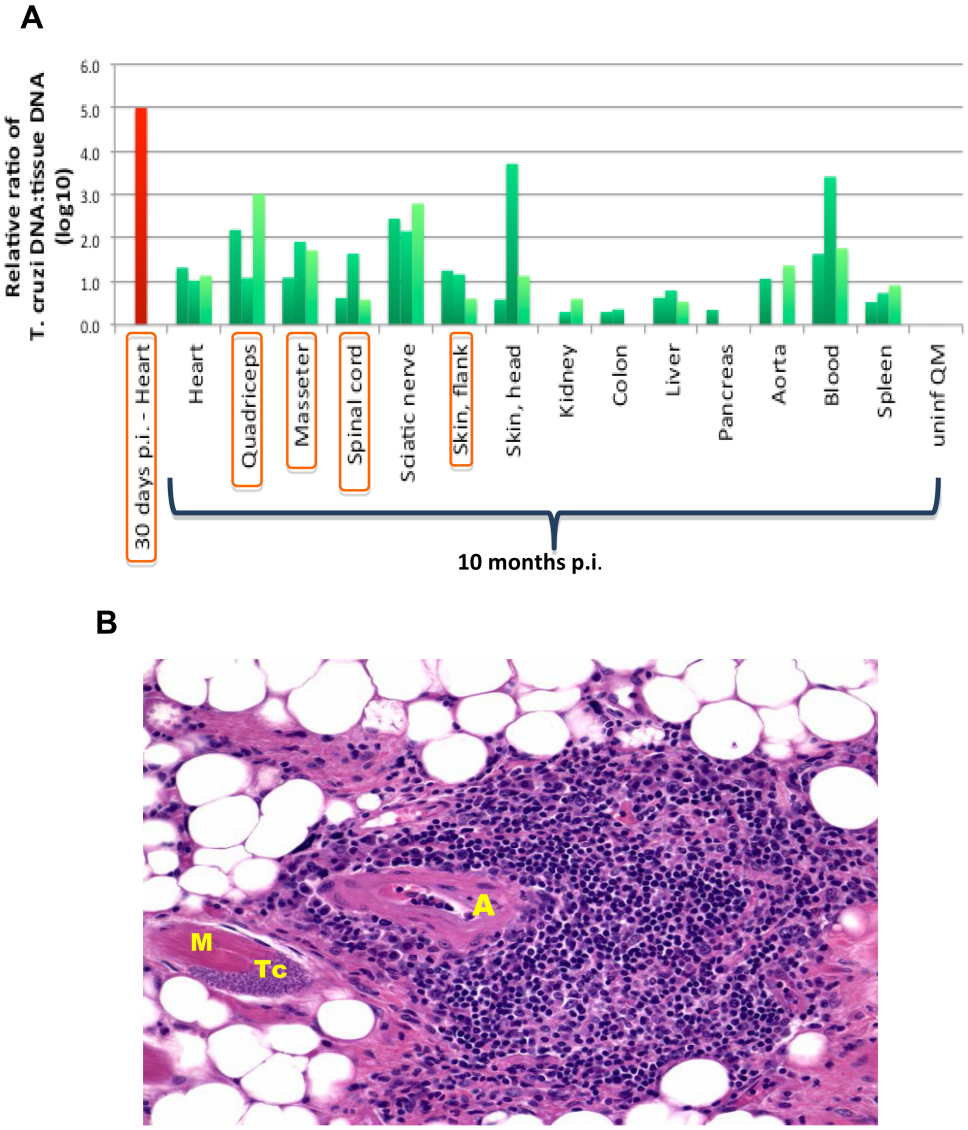

FIG 7 *T. cruzi* is detectable at very low levels in the chronic phase of infection, mainly in organs where systemic necrotizing vasculitis lesions are found. Mice were euthanized at 7 to 12 months p.i. after developing atrophy and/or partial or total paralysis of the posterior limbs. (A) Quantification by real-time PCR of *T. cruzi* DNA in the indicated organs 10 months after infection (green bars). The negative control was a quadriceps muscle taken from an uninfected mouse 10 months after infection of age-matched infected mice, shown at the right (uninf QM), and the positive control was a heart analyzed 30 days after infection (red). Data are shown for 3 mice for each tissue and condition, except for the acutely infected heart ($n = 1$). Rare parasite nests were visualized in all tissues whose names are circumscribed in orange. (B) Amastigote nest in a skeletal muscle myocyte adjacent to vasculitis. By H&E staining, a single parasite nest was found in skeletal muscles from a total of 12 mice analyzed. A, arteriole; M, skeletal muscle myocyte; Tc, *T. cruzi* amastigote nest. Magnification, ×200.

toimmunity, as the mechanism of pathogenesis. Future work will be needed to define the antigen specificity of the remaining 85% of the $CD8^+$ T cells in the skeletal muscle lesions in *T. cruzi*-infected mice, whether they are required to maintain suppression of the parasite during persistent infection, and why they are unable to clear the parasite completely from most tissues. In fact, the presence of $CD8^+$ T cells that may be dysfunctional (with phenotypic markers of effector/memory, such as CD27 and CD28, and the ability to produce IFN-γ) in chronic *T. cruzi* infection in mice (27) and in chagasic patients (28, 29) has been shown to correlate with the severity of disease. It will also be interesting and important in future work to define (i) whether a persistent low level of parasites is required to maintain vasculitis lesions in the model, (ii) how innate and adaptive immune responses in the lesions are coordinated and regulated, (iii) why the immune response is localized mainly to arteries and arterioles, and (iv) the mechanism of fibrinoid necrosis. In PAN, the latter is thought to be the result of neutrophil degranulation, but specific molecular details are lacking (22). It is interesting to speculate that localization of the inflammation to arterioles may be the result of an incomplete chemoattractant relay from blood to tissue that is, on the one hand, sufficiently large to stage immune cells at vessels in infected tissue but, on the other hand, insufficient to trigger robust migration to infected microdomains. In this regard, our immunohistochemical studies showed that the parasite burden was very low in all tissues examined, including skeletal muscle, and that the parasite could

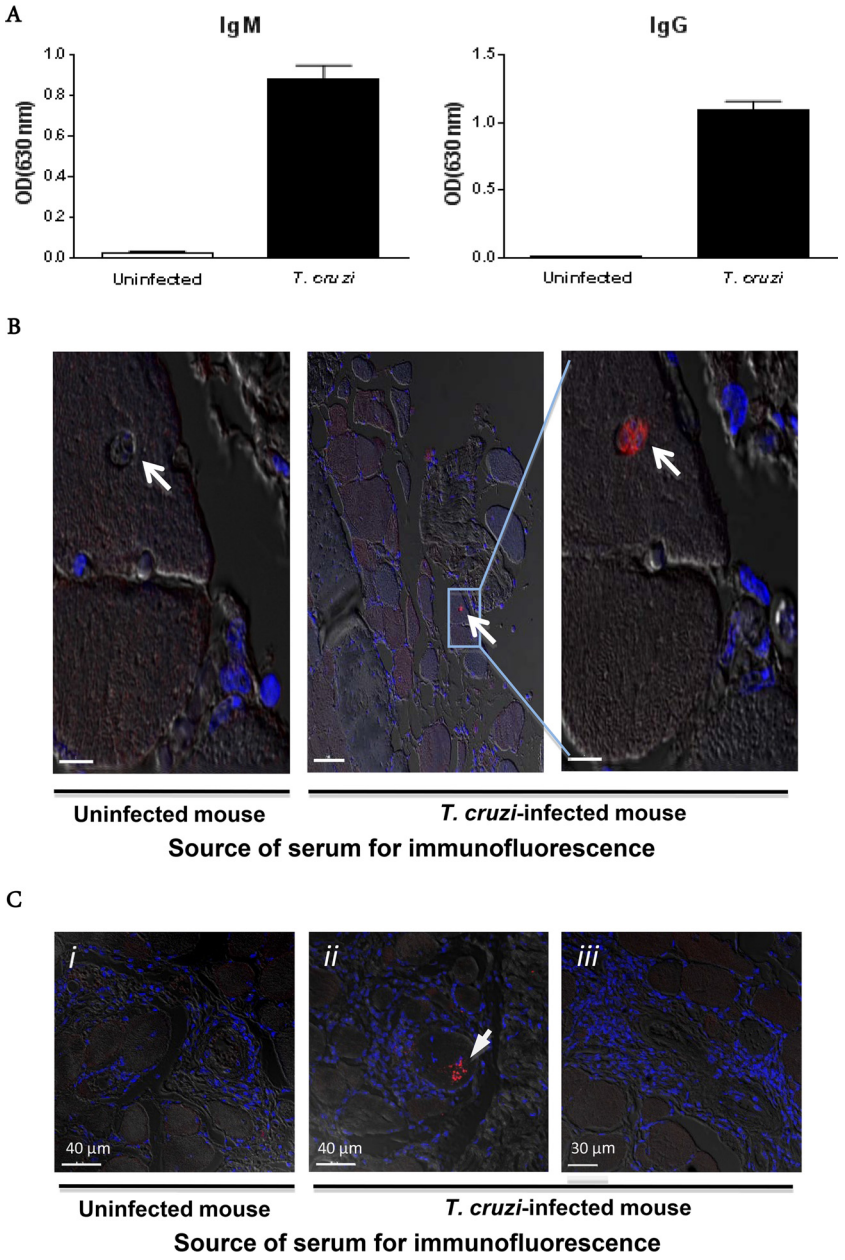

FIG 8 Immune sera identify *T. cruzi* in myocytes *in situ*. (A) Parasite-specific antibody responses in paretic *T. cruzi*-infected mice (10 months p.i.). (B) Immunofluorescence localization of an amastigote nest (white arrow), using serum from a chronically infected mouse. Two serial sections of quadriceps muscle from a paretic *T. cruzi*-infected mouse were stained with either serum from the same mouse or serum from an age-matched uninfected mouse. The results were confirmed on the same tissue with sera from two other chronically *T. cruzi*-infected mice. Bars, 7 μm (left), 50 μm (middle), and 7 μm (right). (C) Absence of antibody deposits in systemic necrotizing vasculitis lesions in skeletal muscle. Sections of quadriceps muscle from a paretic *T. cruzi*-infected mouse were stained with serum from a paretic *T. cruzi*-infected mouse or an age-matched uninfected mouse. Slides were then stained with an anti-mouse IgG secondary antibody (red) and counterstained with DAPI (blue). Confocal immunofluorescence images are superimposed on bright-field images. i and iii, fields with systemic necrotizing vasculitis lesions; ii, *T. cruzi* within a skeletal muscle fiber (the arrow denotes an arteriole).

persist in skeletal muscle myocytes, presumably inducing release of low levels of immunoregulatory cytokines and chemokines as trypomastigotes emerged from myocytes and were attacked and killed by humoral immune mechanisms. This could explain the presence of readily detectable, though low, PCR signals for parasite DNA despite the extreme paucity of visible parasites by microscopy. We never directly observed any parasites within the vasculitis lesions, however.

At the molecular level, we found that type I cytokines (e.g., TNF-α and IFN-γ) and chemokines (e.g., Ccl5 and Cxcl9), as well as chemokine receptors (e.g., Cxcr3 and Ccr2), were upregulated in skeletal muscles from paretic mice. This extends the findings of Sunnemark et al. (7), who reported that TNF-α and IL-6 were associated with inflammatory lesions in the aorta in chronically *T. cruzi*-infected mice. Patients with hepatitis C virus-associated mixed cryoglobulinemia have also been reported to express Th1

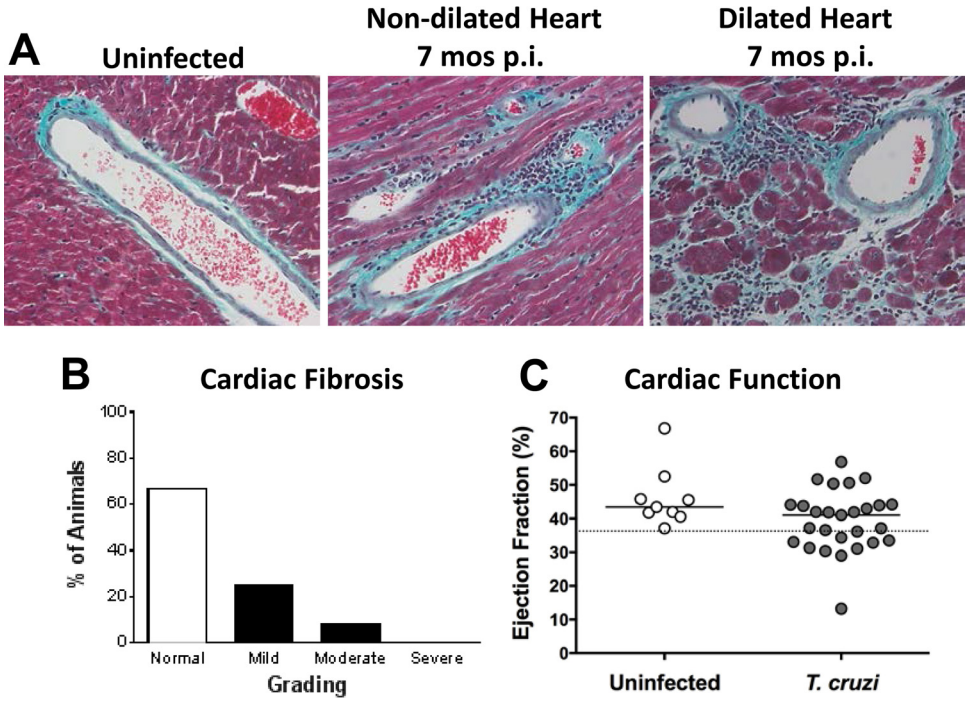

FIG 9 Cardiac fibrosis and dysfunction in chronically *T. cruzi*-infected mice. Mice were analyzed 7 months after infection with *T. cruzi*. (A and B) Gomori's trichrome stain for collagen. Images in panel A are representative of a total of 12 animals whose fibrosis varied in severity, as scored in panel B. Magnification, ×400. (C) Ejection fraction measured by ultrasound of infected or age-matched uninfected control mice. The dotted line represents the lower limit of the 99% confidence interval of ejection fractions for uninfected mice ($P < 0.05$; Fisher's exact test); odds ratios were not statistically significantly different. The solid horizontal lines indicate the medians for the groups analyzed. Data were pooled from 2 independent experiments.

cytokines, including IFN-γ and TNF-α, in vasculitic nerve lesions (30). Chemokines and chemokine receptors involved in T cell and monocyte trafficking, such as Ccl3, Ccl4, and Cxcr3, were also significantly upregulated (30).

The presence of dendritic cells and lymphocytes in human PAN lesions suggests that antigen-specific T cell-mediated immune responses may play a role in its pathogenesis as well. However, the nature of these antigens and whether they are allo- or autoreactive remain unknown (31). Unlike the case for several other vasculitis syndromes, ANCA are typically negative in PAN, and glomerulonephritis and complement consumption are unusual. In addition, PAN stands out among other types of vasculitis by virtue of its association with potential viral triggers, mainly HBV, but also HCV, HIV, cytomegalovirus, and parvovirus B19 (31). In this regard, the chief significance of our study is that in this mouse model, *T. cruzi* is not just associated with systemic necrotizing vasculitis lesions but also causes them.

Future studies will be needed to test whether *T. cruzi* or a related parasite acting by the same or a similar pathogenic mechanism might be responsible for some cases of human vasculitis. The most obvious potential setting would be in patients with Chagas' disease, as a clinical consequence of persistent *T. cruzi* infection in humans, characterized classically by chronic dilated cardiomyopathy and chronic dilated gastroenteropathy. As many as 60% of Chagas' disease patients may have skeletal muscle inflammation (12), involving vasculitis characterized by an accumulation of lymphocytes and macrophages (20); in experimental animals, associated intracellular parasites were rarely found in one study (4) but were observed in 25% of cases in a second study (6). Consistent with this pattern of pathology, cardiac myocytes, neurons, and striated myocytes are all highly susceptible to *T. cruzi* infection (13).

In addition to chagasic cardiomyopathy (32, 33), complications involving the cardiovascular system in Chagas' disease include acute ischemic stroke (34), where the etiology is cardiac thromboembolism in most cases and is cryptogenic in a minority (20 to 25%) (35). Peripheral neuropathy has also been documented for Chagas' disease. Although mostly subclinical, some patients may present with mild sensory-motor findings (36, 37). Our study suggests a revisiting of muscle and nerve pathology in patients with Chagas' disease for evidence of vasculitis.

The factors responsible for triggering and maintaining intense chronic inflammation in Chagas' disease remain poorly defined. Lesion severity correlates with parasite burden or the presence of parasite DNA (38–40); however, in Chagas' disease, as in our mouse model of *T. cruzi*-dependent systemic necrotizing vasculitis, the degrees of inflammation and organ destruction are highly disproportionate to the low parasite burden found in the chronic phase. Whether this level of parasite is sufficient to maintain chagasic immunopathology or instead requires recruitment of autoreactive responses following a parasite-induced break of tolerance is an important unanswered question.

In conclusion, our clinical, histopathological, parasitological, and immunological analyses of chronic vascular disease occurring after *T. cruzi* infection of mice have revealed a picture most consistent with a pathogen-specific, type I cytokine- and $CD8^+$ T cell-driven immunopathogenesis. Future analysis of this model may provide novel insights into mechanisms by which *T. cruzi*

induces the pathology of Chagas' disease, as well as how a pathogen may cause vasculitis in humans. Finally, the model may be useful for identifying novel targets for treatment of vasculitis.

ACKNOWLEDGMENTS

We are grateful to Fuyuki Tokumasu (Laboratory of Malaria and Vector Research, NIAID, NIH) for the kind donation of the Colombiana strain of *T. cruzi*, to the NIH Tetramer Core Facility (contract HHSN272201300006C) for provision of TSKB20 (ANYKFTLV/Kb) tetramers, to Daryl Despres (Mouse Imaging Facility, NIH) for performing the ultrasound measurements, and to Michael A. Eckhaus (Head of Pathology, Diagnostic & Research Services, DVR, NIH) for valuable discussions about the pathology of *T. cruzi* infection. We are also in debt to Katina Thomas and other members of the outstanding technical staff of the NIAID Animal Facility, as well as to Alfonso Gozalo (Facility Veterinarian, Comparative Medicine Branch, NIAID, NIH), for technical support and helpful discussions.

FUNDING INFORMATION

This work was supported by the Division of Intramural Research, National Institute of Allergy and Infectious Diseases, NIH.

REFERENCES

1. **Guillevin L.** 2013. Infections in vasculitis. Best Pract Res Clin Rheumatol **27:**19–31. http://dx.doi.org/10.1016/j.berh.2013.01.004.
2. **van Timmeren MM, Heeringa P, Kallenberg CG.** 2014. Infectious triggers for vasculitis. Curr Opin Rheumatol **26:**416–423. http://dx.doi.org/10.1097/BOR.0000000000000068.
3. **Said G, Joskowicz M, Barreira AA, Eisen H.** 1985. Neuropathy associated with experimental Chagas' disease. Ann Neurol **18:**676–683. http://dx.doi.org/10.1002/ana.410180609.
4. **Gonzalez Cappa SM, Sanz OP, Muller LA, Molina HA, Fernandez J, Rimoldi MT, Sica RE.** 1987. Peripheral nervous system damage in experimental chronic Chagas' disease. Am J Trop Med Hyg **36:**41–45.
5. **Molina HA, Kierszenbaum F.** 1988. Kinetics of development of inflammatory lesions in myocardial and skeletal muscle in experimental *Trypanosoma cruzi* infection. J Parasitol **74:**370–374. http://dx.doi.org/10.2307/3282040.
6. **Losavio A, Jones MC, Sanz OP, Mirkin G, Gonzalez Cappa SM, Muchnik S, Sica RE.** 1989. A sequential study of the peripheral nervous system involvement in experimental Chagas' disease. Am J Trop Med Hyg **41:**539–547.
7. **Sunnemark D, Frostegard J, Orn A, Harris RA.** 1998. Cellular and cytokine characterization of vascular inflammation in CBA/J mice chronically infected with *Trypanosoma cruzi*. Scand J Immunol **48:**480–484. http://dx.doi.org/10.1046/j.1365-3083.1998.00410.x.
8. **Jelicks LA, Chandra M, Shirani J, Shtutin V, Tang B, Christ GJ, Factor SM, Wittner M, Huang H, Weiss LM, Mukherjee S, Bouzahzah B, Petkova SB, Teixeira MM, Douglas SA, Loredo ML, D'Orleans-Juste P, Tanowitz HB.** 2002. Cardioprotective effects of phosphoramidon on myocardial structure and function in murine Chagas' disease. Int J Parasitol **32:**1497–1506. http://dx.doi.org/10.1016/S0020-7519(02)00136-4.
9. **Nagajyothi F, Desruisseaux M, Bouzahzah B, Weiss LM, Andrade Ddos S, Factor SM, Scherer PE, Albanese C, Lisanti MP, Tanowitz HB.** 2006. Cyclin and caveolin expression in an acute model of murine Chagasic myocarditis. Cell Cycle **5:**107–112. http://dx.doi.org/10.4161/cc.5.1.2284.
10. **Okumura M, Brito T, Pereira-da-Silva LH, Carvalho-da-Silva A, Correa-Neto A.** 1960. The pathology of experimental Chagas' disease in mice. I. Digestive tract changes with special reference to necrotizing arteritis. Rev Inst Med Trop São Paulo **2:**17–28.
11. **Dias E, Laranja FS, Miranda A, Nobrega G.** 1956. Chagas' disease; a clinical, epidemiologic, and pathologic study. Circulation **14:**1035–1060. http://dx.doi.org/10.1161/01.CIR.14.6.1035.
12. **Laguens RP, Cossio PM, Diez C, Segal A, Vasquez C, Kreutzer E, Khoury E, Arana RM.** 1975. Immunopathologic and morphologic studies of skeletal muscle in Chagas' disease. Am J Pathol **80:**153–162.
13. **Chagas C.** 1911. Nova entidade morbida do homem: rezumo geral de estudos etiolojicos e clinicos. Mem Inst Oswaldo Cruz **3:**56.
14. **Federici EE, Abelmann WH, Neva FA.** 1964. Chronic and progressive myocarditis and myositis in C3h mice infected with *Trypanosoma cruzi*. Am J Trop Med Hyg **13:**272–280.
15. **Zingales B, Andrade SG, Briones MR, Campbell DA, Chiari E, Fernandes O, Guhl F, Lages-Silva E, Macedo AM, Machado CR, Miles MA, Romanha AJ, Sturm NR, Tibayrenc M, Schijman AG.** 2009. A new consensus for *Trypanosoma cruzi* intraspecific nomenclature: second revision meeting recommends TcI to TcVI. Mem Inst Oswaldo Cruz **104:**1051–1054. http://dx.doi.org/10.1590/S0074-02762009000700021.
16. **Brener Z.** 1962. Therapeutic activity and criterion of cure on mice experimentally infected with *Trypanosoma cruzi*. Rev Inst Med Trop Sao Paulo **4:**389–396.
17. **Roffe E, Rothfuchs AG, Santiago HC, Marino AP, Ribeiro-Gomes FL, Eckhaus M, Antonelli LR, Murphy PM.** 2012. IL-10 limits parasite burden and protects against fatal myocarditis in a mouse model of *Trypanosoma cruzi* infection. J Immunol **188:**649–660. http://dx.doi.org/10.4049/jimmunol.1003845.
18. **Martin DL, Murali-Krishna K, Tarleton RL.** 2010. Generation of *Trypanosoma cruzi*-specific $CD8^+$ T-cell immunity is unaffected by the absence of type I interferon signaling. Infect Immun **78:**3154–3159. http://dx.doi.org/10.1128/IAI.00275-10.
19. **Petkova SB, Tanowitz HB, Magazine HI, Factor SM, Chan J, Pestell RG, Bouzahzah B, Douglas SA, Shtutin V, Morris SA, Tsang E, Weiss LM, Christ GJ, Wittner M, Huang H.** 2000. Myocardial expression of endothelin-1 in murine *Trypanosoma cruzi* infection. Cardiovasc Pathol **9:**257–265. http://dx.doi.org/10.1016/S1054-8807(00)00045-4.
20. **Cossermelli W, Friedman H, Pastor EH, Nobre MR, Manzione A, Camargo ME, Shiroma M.** 1978. Polymyositis in Chagas's disease. Ann Rheum Dis **37:**277–280. http://dx.doi.org/10.1136/ard.37.3.277.
21. **Jennette JC, Falk RJ, Bacon PA, Basu N, Cid MC, Ferrario F, Flores-Suarez LF, Gross WL, Guillevin L, Hagen EC, Hoffman GS, Jayne DR, Kallenberg CG, Lamprecht P, Langford CA, Luqmani RA, Mahr AD, Matteson EL, Merkel PA, Ozen S, Pusey CD, Rasmussen N, Rees AJ, Scott DG, Specks U, Stone JH, Takahashi K, Watts RA.** 2013. 2012 revised International Chapel Hill Consensus Conference nomenclature of vasculitides. Arthritis Rheum **65:**1–11. http://dx.doi.org/10.1002/art.37715.
22. **Cid MC, Grau JM, Casademont J, Campo E, Coll-Vinent B, Lopez-Soto A, Ingelmo M, Urbano-Marquez A.** 1994. Immunohistochemical characterization of inflammatory cells and immunologic activation markers in muscle and nerve biopsy specimens from patients with systemic polyarteritis nodosa. Arthritis Rheum **37:**1055–1061. http://dx.doi.org/10.1002/art.1780370711.
23. **Garcia F, Pedrol E, Casademont J, Mellado B, Cordoba R, Cid M, Grau JM.** 1992. Polyarteritis nodosa confined to calf muscles. J Rheumatol **19:**303–305.
24. **Kamimura T, Hatakeyama M, Torigoe K, Nara H, Kaneko N, Satou H, Yoshio T, Okazaki H, Minota S.** 2005. Muscular polyarteritis nodosa as a cause of fever of undetermined origin: a case report and review of the literature. Rheumatol Int **25:**394–397. http://dx.doi.org/10.1007/s00296-004-0531-4.
25. **Plumley SG, Rubio R, Alasfar S, Jasin HE.** 2002. Polyarteritis nodosa presenting as polymyositis. Semin Arthritis Rheum **31:**377–383. http://dx.doi.org/10.1053/sarh.2002.32549.
26. **Pagnoux C, Seror R, Henegar C, Mahr A, Cohen P, Le Guern V, Bienvenu B, Mouthon L, Guillevin L.** 2010. Clinical features and outcomes in 348 patients with polyarteritis nodosa: a systematic retrospective study of patients diagnosed between 1963 and 2005 and entered into the French Vasculitis Study Group Database. Arthritis Rheum **62:**616–626. http://dx.doi.org/10.1002/art.27240.
27. **Leavey JK, Tarleton RL.** 2003. Cutting edge: dysfunctional CD8+ T cells reside in nonlymphoid tissues during chronic *Trypanosoma cruzi* infection. J Immunol **170:**2264–2268. http://dx.doi.org/10.4049/jimmunol.170.5.2264.
28. **Albareda MC, Laucella SA, Alvarez MG, Armenti AH, Bertochi G, Tarleton RL, Postan M.** 2006. Trypanosoma cruzi modulates the profile of memory CD8+ T cells in chronic Chagas' disease patients. Int Immunol **18:**465–471. http://dx.doi.org/10.1093/intimm/dxh387.
29. **Laucella SA, Postan M, Martin D, Hubby Fralish B, Albareda MC, Alvarez MG, Lococo B, Barbieri G, Viotti RJ, Tarleton RL.** 2004. Frequency of interferon-gamma-producing T cells specific for *Trypanosoma cruzi* inversely correlates with disease severity in chronic human Chagas disease. J Infect Dis **189:**909–918. http://dx.doi.org/10.1086/381682.
30. **Saadoun D, Bieche I, Maisonobe T, Asselah T, Laurendeau I, Piette JC, Vidaud M, Cacoub P.** 2005. Involvement of chemokines and type 1 cytokines in the pathogenesis of hepatitis C virus-associated mixed cryo-

globulinemia vasculitis neuropathy. Arthritis Rheum **52:**2917–2925. http://dx.doi.org/10.1002/art.21270.
31. **Hernandez-Rodriguez J, Alba MA, Prieto-Gonzalez S, Cid MC.** 2014. Diagnosis and classification of polyarteritis nodosa. J Autoimmun **48–49:** 84–89. http://dx.doi.org/10.1016/j.jaut.2014.01.029.
32. **Rossi MA, Goncalves S, Ribeiro dos Santos R.** 1984. Experimental *Trypanosoma cruzi* cardiomyopathy in BALB/c mice. The potential role of intravascular platelet aggregation in its genesis. Am J Pathol **114:**209–216.
33. **Factor SM, Cho S, Wittner M, Tanowitz H.** 1985. Abnormalities of the coronary microcirculation in acute murine Chagas' disease. Am J Trop Med Hyg **34:**246–253.
34. **Carod-Artal FJ, Gascon J.** 2010. Chagas disease and stroke. Lancet Neurol **9:**533–542. http://dx.doi.org/10.1016/S1474-4422(10)70042-9.
35. **Carod-Artal FJ, Vargas AP, Melo M, Horan TA.** 2003. American trypanosomiasis (Chagas' disease): an unrecognised cause of stroke. J Neurol Neurosurg Psychiatry **74:**516–518. http://dx.doi.org/10.1136/jnnp.74.4.516.
36. **Genovese O, Ballario C, Storino R, Segura E, Sica RE.** 1996. Clinical manifestations of peripheral nervous system involvement in human chronic Chagas disease. Arq Neuropsiquiatr **54:**190–196.
37. **Said G.** 2007. Infectious neuropathies. Neurol Clin **25:**115–137. http://dx.doi.org/10.1016/j.ncl.2006.11.004.
38. **Zhang L, Tarleton RL.** 1999. Parasite persistence correlates with disease severity and localization in chronic Chagas' disease. J Infect Dis **180:**480–486. http://dx.doi.org/10.1086/314889.
39. **Palomino SA, Aiello VD, Higuchi ML.** 2000. Systematic mapping of hearts from chronic chagasic patients: the association between the occurrence of histopathological lesions and *Trypanosoma cruzi* antigens. Ann Trop Med Parasitol **94:**571–579.
40. **Benvenuti LA, Roggerio A, Freitas HF, Mansur AJ, Fiorelli A, Higuchi ML.** 2008. Chronic American trypanosomiasis: parasite persistence in endomyocardial biopsies is associated with high-grade myocarditis. Ann Trop Med Parasitol **102:**481–487. http://dx.doi.org/10.1179/136485908X311740.